https://doi.org/10.22226/2410-3535-2022-4-409-413

Effect of strain of cryorolling on structure and strength of nickel

M. V. Markushev†, I. Sh. Valeev, E. V. Avtokratova, R. R. Ilyasov,
A. Kh. Valeeva, S. V. Krimsky, O. Sh. Sitdikov
†mvmark@imsp.ru

Institute for Metals Superplasticity Problems, RAS, Ufa, 450001, Russia

The effect of isothermal rolling at liquid nitrogen temperature with reductions up to 90% on the structural-mechanical behavior of coarse-grained nickel was evaluated by TEM, SEM-EBSD and X-ray analysis methods, and microhardness measurements. The highest hardening rate of the metal was found at the initial stage of rolling (up to about 50%), after which it decreased slightly with further reductions. Detailed analyses of the evolution of dislocation density, grain size and grain boundary spectra have shown that the behavior found was attributed to an extremely low deformation temperature, resulted in a decreased rate of accumulation of crystalline defects, as well as the formation and rearrangement of dislocation structure. Due to the strong suppression of dynamic recovery and recrystallization, even when rolling to a reduction of 90%, a relatively homogeneous coarse-fibered structure with a developed nanocellular substructure and less than 5% fraction of nanoscale dynamically recrystallized grains was formed. It was concluded that the main structural strengthening factors in cryogenically rolled nickel was the formation of low-energy dislocation structures and their transformations into a well-developed substructure with nanosized crystallites separated predominantly by low-angle boundaries.

Keywords: nickel, cryogenic rolling, structure, hardness.

1. Introduction

Cryogenic deformation temperatures (below 120 K (–153°C)) [1] are the basis of a number of thermomechanical treatment (TMT) routes of metals and alloys with the aim to impart them ultrafine grained and even nanocrystalline structure with crystallite (grain/subgrain) size less than 1 and 0.1 μm, respectively. The reason for the quite high interest in such processing arises from the well-known conception that the lower the deformation temperature, the stronger the resulting material. The latter is due to the higher suppression of dynamic recovery with decreasing strain temperature, which leads to a greater accumulation of crystal defects and an increase in the internal stresses of crystal lattices [2 – 6]. In addition, these processes can lead to stronger structural strengthening due to stronger refinement of crystallites surrounded by both low-angle and high-angle boundaries (LABs and HABs), which is most relevant when the so-called severe plastic deformation (SPD) with true strain above 1 is realized [4 –11]. It should be noted that SPD involving TMT can activate not only dynamic but also static grain/subgrain refinement, which occur under deformation and subsequent post-deformation heat treatment, respectively. In this case, one of the most crucial points for the optimal structuring and hardening the material processed, and, consequently, the semi-finished and final products, are the conditions of their deformation. For cryorolling (CR), however, this point is not yet so clear, even for pure metals and low-alloy systems, especially in terms of a thorough analysis of the evolution of their structure, as well as the structure-strength relationships [4,11,12].

Thus, the purpose of the present study was to investigate, using a number of powerful methods of metallographic analysis, the phenomenology and nature of changes in structure and strength of pure nickel caused by isothermal cryogenic rolling in a wide strain range.

2.Material and methods

Studies were carried out on a NP2-grade nickel ingot that was pre-setted at 850°C to a strain of $\varepsilon \approx 70\%$ and annealed at 600°C for 2 hours. The subsequent deformation of mechanically cut sheet blanks to $\varepsilon = 30, 50, 70$ and 90% ($e = 0.3, 0.7, 1.2$ and 2.3, respectively) was carried out by multi-pass isothermal rolling at a temperature of liquid nitrogen in a laboratory six-roll mill. The dimensions of the blanks were selected so that their final thickness after each rolling reduction implemented was equal to 0.4 mm. Isothermal conditions of CR were provided by a preliminary 1 hour soaking of blanks and removable working rolls in liquid nitrogen. During rolling the blanks were immersed in nitrogen after each pass and the rolls after 5 passes. The strain per pass did not exceed 7%, the rolling rate was about 100 mm/min.

The microstructure of Ni was studied in the setting/rolling plane using a TESCAN MIRA 3 LMH scanning electron microscope (SEM), equipped with EBSD analyzer and HKL Channel 5 software. Diffraction patterns were analyzed by 6 Kikuchi lines at scanning steps of 0.1 and 0.5 μm. A misorientation angle of 15° was considered as the criterion for separating LABs and HABs. The mean sizes of grains and subgrains, d_g and d_{sg}, were determined as their equivalent

diameters. At that, the subgrains were separated from neighbor crystallites by both LABs and HABs, in distinction from grains, separated by HABs only. The average misorientation angle of crystallite boundaries, Θ, and the fractions of high-angle and twin boundaries, F_{HABs} and F_{Σ}, were derived from grain boundary diagrams in which boundaries of $\Theta < 2°$ were not taken into account. The fraction of recrystallized grains, F_{rec}, was calculated from the same maps as the ratio of areas of recrystallized and all grains. Crystallites were considered as recrystallized grains in the case of an internal distortion angle of less than 2° (1° for low-scale maps). The majority of the structure parameters mentioned was determined with an accuracy not exceeding 5%.

Transmission electron microscopy (TEM) was performed by a JEOL-2000EX microscope. Specimens for SEM and TEM analyses were processed via the standard procedure of mechanical grinding and polishing, followed by electropolishing at room temperature in a Tenupol-5 twin-jet unit and in a solution of 10% $HClO_4$ and 90% C_4H_9OH.

X-ray diffraction analysis was performed on a DRON-4-07 diffractometer in Cu-K_α radiation at a voltage of 40 kV and a current of 30 mA with a wavelength λ=1.54418 Å. The scanning was performed on rotating sample at a step of 0.1° and an exposure time of 4 sec, and a graphite monochromator on a diffracted beam. The root mean square microdeformation of the crystal lattice, $<\varepsilon^2>^{1/2}$, as well as the coherent domain size, *D*, were estimated by the full-profile method and the MAUD software with an error not exceeding 0.001% and 5 nm, respectively. Dislocation density, ρ, was determined from equation

$$\rho = 2\sqrt{3}\left\langle \varepsilon^2 \right\rangle^{\frac{1}{2}} / \left(D \times b\right),$$

where *b* is the Burgers vector.

Microhardness was determined by the Vickers method on an MVDM 8 "AFFRY" digital tester at a load of 0.5 N and a time of 10 sec. At least ten measurements were performed on each point to obtain an error of no more than 5%.

3. Results and discussions

Judging by the data in Figs. 1 and 2, and Table 1, the initial coarse grains, containing mainly annealing twins, elongated in the rolling direction with strain and acquired a pancake shape. Simultaneously, the density of lattice dislocations increased (Figs. 2 and 3, Table 1), leading to their continuous interaction and formation of the deformation structures consisting of cells, dense dislocation walls and (micro)shear bands, which constituted a network of LABs. The selected area diffraction (SAD) patterns in Fig. 3, showing mostly point-wise reflections, also indicated that the structure in the early stages of CR consisted mainly of crystallites surrounded by low-angle boundaries. With further straining, the reflections tended to stretch azimuthally and transform to the Debye rings, suggesting development of more misoriented structures. Besides, many diffraction points with streaks in the SAD patterns indicated also the development of quite large internal stresses. The latter is in a good agreement with the X-ray determined high dislocation densities and high microstraining of the lattice (Table 1), being always conditioned by the severe straining under decreasing rate of dynamic recovery.

Another related process, as follows from the results of SEM, TEM, and X-ray analyses, was continuous dynamic recrystallization [13–15], which proceeded selectively and encompassed preferentially the areas adjacent to the initial grain boundaries, as sites of shear bands crossing and interaction with grain boundaries (as arrowed in Fig. 2). However, the impact of recrystallization on the structure transformations of the Ni resulting in grain refinement via initial grain fragmentation and new fine grain formation was insignificant (Figs. 2 and 3). After CR, even with a maximum reduction up to 90%, the fractions of both HABs and recrystallized grains were too low (Fig. 4 and Table 1). Therewith, the sizes of subgrains and coherent domains decreased gradually with strain and reached about 200 and 70 nm, respectively, while the recrystallized grains were one order of magnitude larger than the subgrains.

Besides, the early CR stage was accompanied by a sharp decrease in the fraction of twin boundaries present in the initial structure (Fig. 1, Table 1), which can be discussed as follows. It is known that the deformation twinning does not occur in coarse-grained face-centered cubic metals with high stacking-fault energy, γ [16]. A typical example is Al with $\gamma = 300$ erg/cm^2 [16,17]. In contrast, twinning at room temperature straining may be a significant phenomenon in copper and its alloys [18,19], which are typical representatives of materials with low stacking-fault energy (γ for Cu is only about 50 erg/cm^2 [17]), especially when shock-strengthening

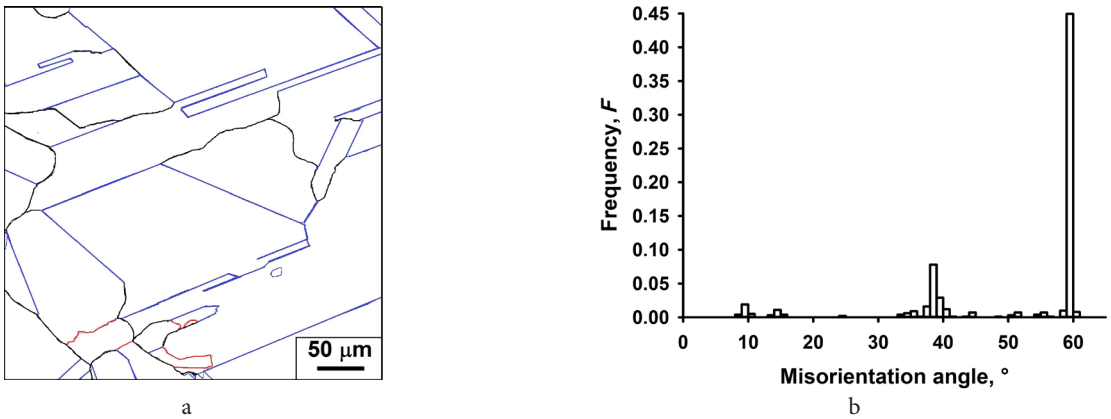

a b

Fig. 1. (Color online) SEM-EBSD map (a) and grain boundary spectrum (b) in Ni before cryorolling. Here and after black, red and blue lines indicate HABs, LABs and twin boundaries, consequently.

Table 1. Microstructure parameters of Ni before and after cryorolling.

Strain, %	d_{sg}, μm	d_g, μm	F_{rec}, %	F_{HABs}, %	Θ, deg.	F_{Σ}, %	Lattice parameter, Å	ρ, 10^{13} m^{-2}	D, nm	$<\varepsilon^{1/2}>$, %
0	-	250	-	94	54	42	3.515 ± 0.001	0.3	558 ± 4	-
30	0.3	-	0	7	7	0.6	3.514 ± 0.001	9	152 ± 3	0.094 ± 0.003
50	0.3	2.9	1	4	5	0.2	3.513 ± 0.001	24	75 ± 2	0.126 ± 0.003
70	0.2	3.3	3	5	6	0.1	3.513 ± 0.001	30	72 ± 4	0.121 ± 0.005
90	0.2	2.5	3	7	7	0.2	3.512 ± 0.001	35	68 ± 4	0.165 ± 0.002

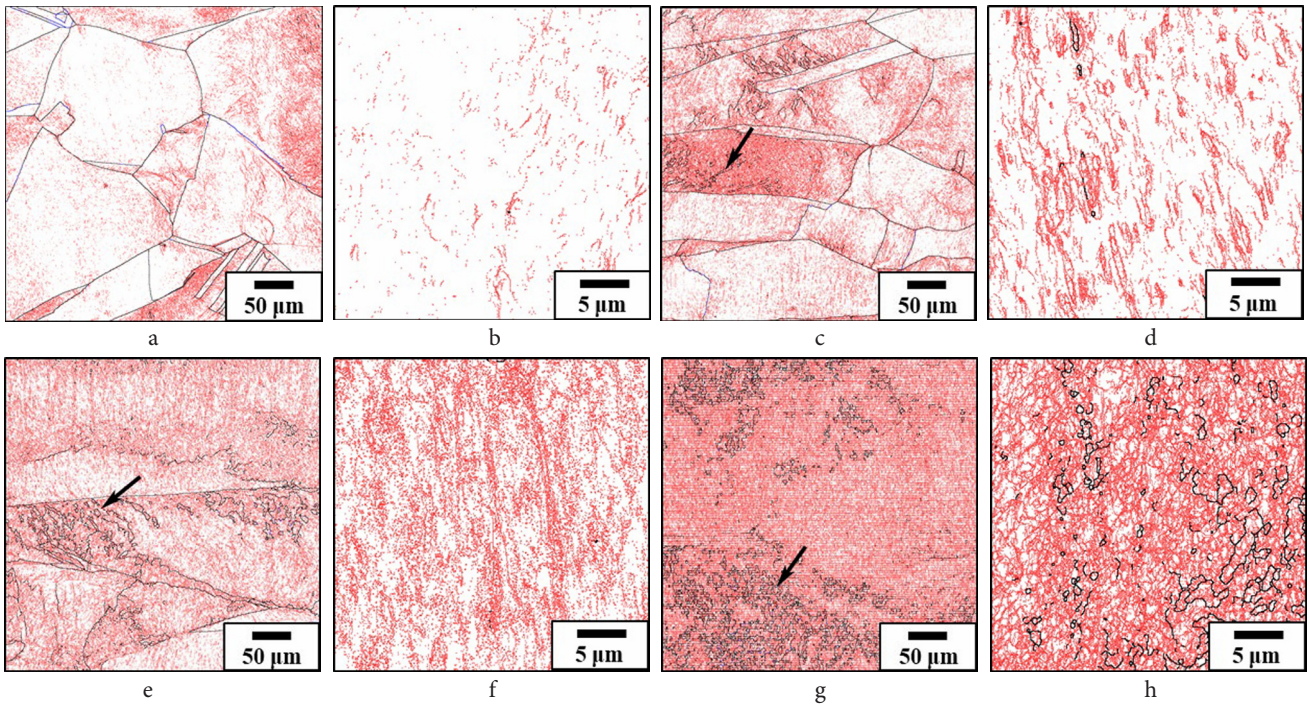

Fig. 2. (Color online) SEM-EBSD maps for Ni after CR with a strain of 30 (a, b), 50 (c, d), 70 (e, f) and 90% (g, h) (rolling direction is horizontal). In Fig. b, d, f, and h, LABs start from 1 degree.

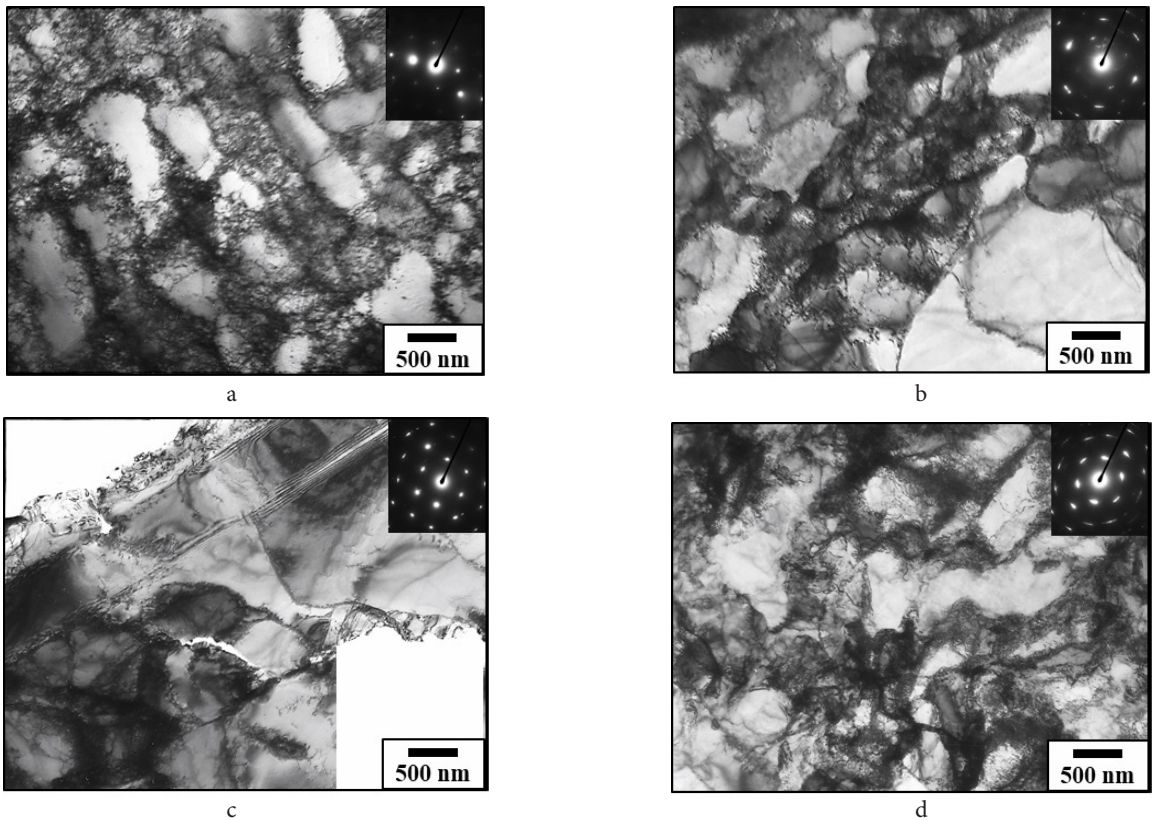

Fig. 3. TEM structures of Ni cryorolled to a strain of 30 (a), 50 (b), 70 (c) and 90% (d). Diffraction patterns were obtained from an area about 12 $μm^2$.

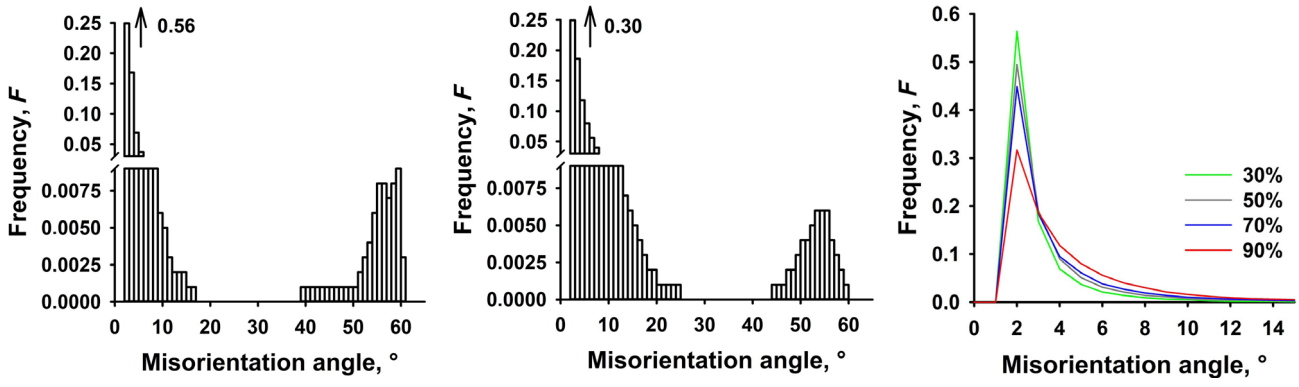

Fig. 4. (Color online) Boundary spectra in Ni cryorolled to 30 (a) and 90% (b) and their low-angle part after CR with different strains (c).

increased upon deformation. At the same time, it was found that mechanical twinning does not practically occur during cryorolling of Cu [11]. The data represented in Table 1 indicated in turn that pure nickel, which occupies an intermediate position in terms of stacking-fault energy ($\gamma = 200$ erg/cm^2 [17]), also does not undergo mechanical twinning during CR, whereas twin formation takes place during pre-treatment annealing. This suggested that the initial annealing twins could be involved in the structural changes during cryorolling, contributing to the development of new grains [20,21].

As can be seen in Fig. 4 a,b, along with the formation of HABs with relatively low angles ranging between 15 and 20°, the misorientation spectra at all strains studied retained actual peaks at 50 – 60°, which inherited from the initial structure (Fig. 1) and approximately corresponded to the Σ3 twin boundaries within the Brandon criterion (±8.7° [21]). In accordance with the mechanism described elsewhere [20], the twin boundaries are changed to random HABs due to their interaction with moving lattice dislocations and accumulation of orientation misfit dislocations in these boundaries. Note that along with the transformation of LABs into HABs due to continuous dynamic recrystallization, this "twin" dynamic recrystallization mechanism can be a main source of development of HABs and new fine grains during CR.

On the other hand, due to the lack of changes in the type of boundary spectra (Fig. 4) and their average misorientation angles (Table 1), insignificant fractions of strain-induced HABs, including twin boundaries, were formed at CR. This indicates the non-dominant role of the dynamic recrystallization in the Ni structural development. Therewith, it can be generally argued that the main structural transformations occurring during cryorolling of Ni were originated from the evolution of dislocation structures under conditions of low rate of dynamic recovery.

According to the microstructure analysis, cryostraining of the Ni resulted in accumulation of dislocations mainly in the walls, forming cells, whose size continuously decreased with an insignificant increase in their misorientations (Figs. 2 – 4, Table 1). The latter, in turn, usually expressed in the absence of a steady stage of deformation, and is well presented in Fig. 5. Indeed, in the strain range studied, two stages of continuous strengthening with differed intensities can be found. The observation of both, being dislocation-induced in origin,

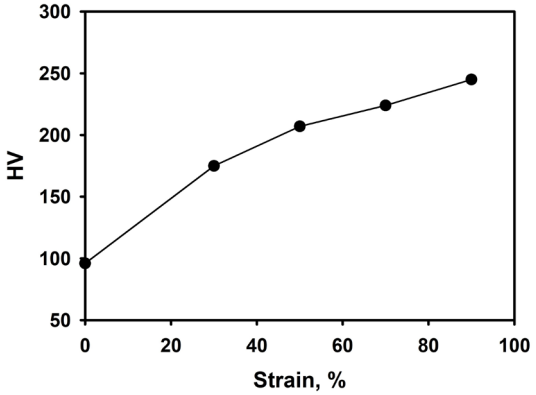

Fig. 5. Dependence of the Ni hardness vs cryorolling strain.

is determined by the main modes of dislocation reactions occurring at each stage of CR. Thus, at straining up to 50% the highest metal hardening effect was accompanied by the development of the highest dislocation density in the form of dislocation walls, i.e. cell- and band boundaries (Fig. 3 a,b). Further, but much slower strengthening was occurred due to another character of the matrix restructuring. Judging by the evolution of few factors, involving the intensity and uniformity of LABs "red" contrast in Fig. 2, reduction in the cell size (Table 1) and the most prominent transformations of grain boundary spectra in the low-angle range (Fig. 4 c), it could be concluded that at high strains, the rearrangement of substructure and continuous increase in its homogeneity preferably took place.

It is worthy to note in this way that the strain-induced dislocation structures are rather diffuse and nonequilibrium interfaces (see Fig. 3 a,b). Dynamic recovery, which occurs with a low rate at cryogenic temperature is unlikely to facilitate the fast transformation of such configurations, involving LABs, to more equilibrium ones [13,14]. However, the deformation to larger strains can give ample time to rearrange dislocations over short distances in a deformation-induced structure, resulting in both increased misorientations and decreased dislocation densities in the boundaries and interiors of crystallites (Fig. 3). By the way it has been also shown [14,22 – 25], that thermal activation via dynamic recovery can be crucial for the development of ultrafine grained structures during cold SPD. This is due to the fact that the transformation of low-angle boundaries into high-angle ones is controlled by the rate of recovery. Thus,

structuring of the Ni at CR is governed by dynamic formation of non-equilibrium boundaries at early stages of deformation and operation of dynamic recovery in these boundaries at higher straining.

So, it can be stated that the nature of structuring in the CR Ni was the formation of low-energy dislocation structures, and their evolution into a well-developed substructure with nanoscale, mainly lightly misoriented crystallites. And the reason for the continuous strengthening of Ni was the strong suppression of dynamic recovery and recrystallization, which led to the predominant formation and development of a dislocation-cellular structure with nanosized coherent domains. At the same time, the effect of recrystallization was insignificant, as the metal behavior was controlled by the processes akin to polygonization.

4. Conclusions

1. Isothermal cryorolling of pure coarse-grained Ni at liquid nitrogen temperature led to its continuous more than twofold hardening with maximum intensity at the initial stage of deformation up to about 50% reduction.

2. Even at strains up to 90%, fragmentation and dynamic recrystallization scarcely occurred and played a minor role in the evolution of Ni structure and strength. As a result, a coarse-fiber structure with a developed nanocellular substructure and an extremely small number of dynamically recrystallized fine grains was formed.

3. The main strengthening mechanism of Ni during cryorolling was conditioned by a sharp increase in dislocation density and the formation of low-misoriented dislocation/cellular structures.

Acknowledgements. The work was supported by the Ministry of Science and Higher Education of Russian Federation through the state assignment of IMSP RAS. It was performed using the facilities of the shared services center "Structural and Physics-Mechanical Studies of Materials" at the Institute for Metals Superplasticity Problems of Russian Academy of Sciences.

References

1. GOST 21957-76. Interstate standard. Cryogenic engineering. Terms and definitions. Moscow, Standartinform (2005) 7 p.
2. Y. Huang, P.B. Prangnell. Acta Mater. 56, 1619 (2008). Crossref
3. T. Konkova, S. Mironov, A. Korznikov, S.L. Semiatin. Acta Mater. 58, 5262 (2010). Crossref
4. E. Ma. JOM. 58, 49 (2006). Crossref
5. S. Krymskiy, O. Sitdikov, E. Avtokratova, M. Markushev. Trans. Nonfer. Met. Soc. of China (English Edition). 30 (1), 14 (2020). Crossref
6. K. Edalati, A. Bachmaier, V. A. Beloshenko, Y. Beygelzimer, V. D. Blank, W. J. Botta, et al. Mater. Res. Lett. 10 (4), 163 (2022). Crossref
7. J. Yin, J. Lu, H. Ma, P. Zhang. J. Mater. Sci. 39, 2851 (2004). Crossref
8. P.B. Prangnell, Y. Huang. J. Mater. Sci. 43, 7280 (2008). Crossref
9. K. Edalati, J.M. Cubero-Sesin, A. Alhamidi, I.F. Mohamed, Z. Horita. Mater. Sci. Eng. A. 613, 103 (2014). Crossref
10. L. Voronova, M. Degtyarev, T. Chashchukhina, T. Gapontseva, V. Pilyugin. Lett. Mater. 8 (4), 424 (2018). Crossref
11. M. Markushev, I. Valeev, A. Valeeva, R. Ilyasov, E. Avtokratova, S. Krymskiy, O. Sitdikov. Facta Univers. Ser.: Mech. Eng. On-Line. (08.2022). Crossref
12. I. Sabirov, M.Yu. Murashkin, R.Z. Valiev. Mater. Sci. Eng. A. 560, 1 (2013). Crossref
13. F.J. Humphreys, M. Hatherly. Recrystallization and Related Annealing Phenomena, 2nd ed. Elsevier, Amsterdam (2004) 658 p. Crossref
14. C. Kobayashi, T. Sakai, A. Belyakov, H. Miura. Phil. Mag. Letters. 87 (10), 751 (2007). Crossref
15. T. Sakai, H. Miura, X. Yang. Mater. Sci. and Eng. A. 499 (1-2), 2 (2009). Crossref
16. M.Y. Gutkin. Nanostructured Metals and Alloys. Processing, Microstructure, Mechanical Properties and Applications. A volume in Woodhead Publishing Series in Metals and Surface Engineering. Woodhead Publishing (2011) pp. 329 – 374. Crossref
17. Sh. Sh. Ibragimov, V.F. Reutov. Radiation defects in metals. Alma-Ata, Nauka (1988) pp. 3 – 24. (in Russian)
18. A. Rohatgi, K.S. Vecchio, G.T. Gray. Metall. Mater. Trans. A. 32 (1), 135 (2001). Crossref
19. A. Rohatgi, K.S. Vecchio, G.T. Gray. Acta Mater. 49 (3), 427 (2001). Crossref
20. O. Sitdikov, R. Kaibyshev, T. Sakai. Mater. Sci. Forum. Trans Tech Publications, Ltd. (2003) pp. 521– 526. Crossref
21. G. Salishchev, S. Mironov, S. Zherebtsov, A. Belyakov. Mater. Phys. and Mech. 25, 42 (2016). (in Russian)
22. I. Mazurina, T. Sakai, H. Miura, O. Sitdikov, R. Kaibyshev. Mat. Trans. 50 (1), 101 (2009). Crossref
23. O. Sitdikov, E. Avtokratova, T. Sakai. J. Alloys Compd. 648, 195 (2015). Crossref
24. O.S. Sitdikov, E.V. Avtokratova, B.I. Atanov, M.V. Markushev. Inorg. Mater. 58, 544 (2022). Crossref
25. I.S. Valeev, A.K. Valeeva, R.R. Ilyasov, O.S. Sitdikov, M.V. Markushev. Lett. Mater. 9 (4), 447 (2019). Crossref